Monomer structures and properties

Molecular structures of each studied base compound are presented in Figure S1. Ammonia, methylamine, dimethylamine and trimethylamine form a homologous series, where the substitution of H by CH_3 increases from zero for amm to three for tma. Thus, in a similar manner, the capability to form hydrogen bonding decreases from four for amm to one for tma. Trimethylamine oxide is an oxidation product of tma, in which an oxygen atom is attached to the nitrogen atom. Structurally tmao resembles tma with three methyl groups, an ability to form only one hydrogen bond and having a C_{3v} symmetry. However, their structures have a substantial differences due to the zwitterionic bond between N^+ and O^-, which cause an immense dipole moment of 5.2 D for tmao, whereas the dipole moment of tma is substantially lower at 0.7 D.

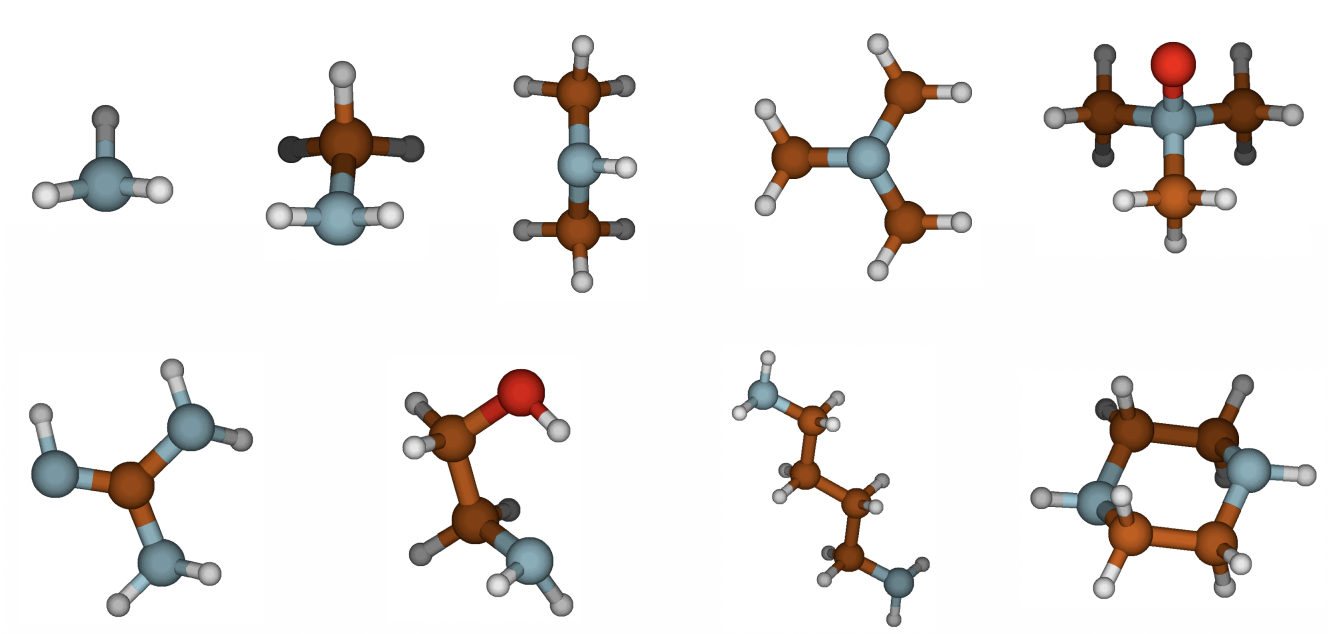

Figure S1. Molecular structures of ammonia, methylamine, dimethylamine, trimethylamine, trimethylamine oxide, guanidine, monoethanolamine, putrescine and piperazine, respectively. Color coding: blue is nitrogen, brown is carbon, red is oxygen and white is hydrogen.

Guanidine has three functional groups: one imino group and two amino groups. When the imino group accepts a proton, there are three identical amino groups and these amino groups are not as basic as amines, since the imino group carbon already carries a positive charge, meaning that gua is very unlikely to accept more than one proton and it is not a triamine. Guanidine can form six hydrogen bonds and has a moderately high dipole moment of 3.0 D. Monoethanolamine, putrescine and piperazine have two functional groups: mea has one amino and one hydroxyl group, and put and pz have two amino groups. The alkanolamine, mea, has an increased ability to form H-bonds compared to monoamines due to the OH group. The primary amino group can form three H-bonds and the hydroxyl group increases the total number of hydrogen binding sites to five. The diamines, put and pz, have an ability to accept two protons. Putrescine has two primary amino groups, both of which can form three H-bonds, making the total number of H-bonds six. Piperazine is has two secondary amino groups in a six-membered ring structure in which both have two hydrogen binding sites and the total number of H-bonds is four. Both put and pz belong to point group of C_i, and therefore, their dipole moment is 0 D. Table S1 lists the dipole moments, polarizabilities, and point groups for monomeric structures. In addition, vapor pressures for the nine bases are listed in Table S2 along with their corresponding sources.

Table S1. Dipole moment, polarizability and point group for neutral and ionic structures.

BASE	Dipole D (neutral)	Dipole D (cation)	Polarizability Å^3 (neutral)	Polarizability Å^3 (cation)	Point group neutral	Point group cation
amm	1.8	0.0	1.6	1.1	C_{3v}	T_d
ma	1.5	2.3	3.3	2.7	C_s	C_{3v}
dma	1.1	1.6	5.2	4.3	C_s	C_2
tma	0.7	0.9	7.1	5.9	C_{3v}	C_{3v}
tmao	5.2	2.1	7.7	6.6	C_{3v}	C_s
gua	3	0.0	5.7	4.7	C_1	D_{3h}
mea	3.4	3.6	5.7	5.0	C_1	C_1
put	0	3.7	9.8	8.9	C_i	C_1
pz	0	4.0	9.3	8.3	C_i	C_s
ACID	neutral	anion	neutral	anion	neutral	anion
sa	3.3	2.7	4.9	5.6	C_2	C_s
msa	3.7	4.2	6.1	7.1	C_s	D_{3h}
na	2.6	0.0	3.4	4.1	C_1	C_{3v}

Table S2. Literature vapor pressure values used in this study.

Base	Vapor Pressure (atm)	Reference
amm	9.8142303	Stull (1947)
ma	3.486597	Aston et al. (1937)
dma	2.044955	Aston et al. (1939)
tma	2.188	Swift and Hochanadel (1945)
tmao	7.41E-10	EPISUITE v. 4.11
gua	0.0028947	EPISUITE v. 4.11
mea	0.0003533	Matthews et al. (1950)
put	0.0031	EPISUITE v. 4.11
pz	0.00094	EPISUITE v. 4.11

We have performed the Gibbs free energy calculations by letting the monomer structures relax toward correct symmetry and making the frequency calculation for the optimized structure for which the quantum chemistry program has detected the point group shown in Table S1. Approximately the same results can be reached by using initially C_1 symmetry for a system and making an *ad hoc* correction to the Gibbs free energy as suggested by Besel et al. (2020). An *ad hoc* correction to the free energy can be calculated as

$$C_{\text{symm}} = RT \ln \sigma_{\text{R}}, \tag{1}$$

where R is the gas constant, T is temperature and σ_{R} is the rotational symmetry number (which is less than or equal to the total symmetry number σ_{tot}).

Methanesulfonic acid and nitric acid complexes

Figure S2 presents the molecular structures of msa–base and na–base heterodimers and their thermochemical parameters are listed in Table S3.

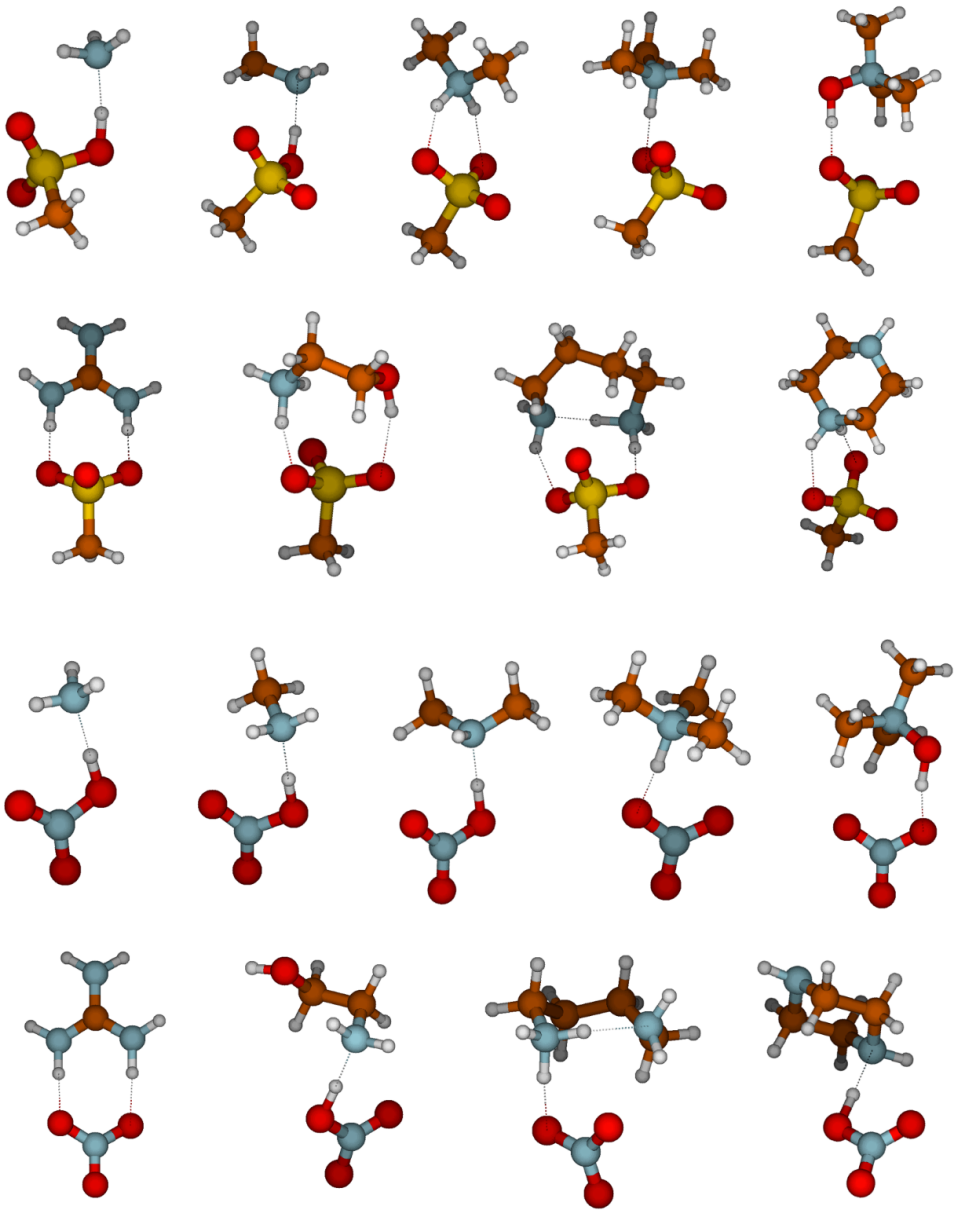

Figure S2. Heterodimers of methanesulfonic acid (top) and nitric acid (bottom) with ammonia, methylamine, dimethylamine, trimethylamine, trimethylamine oxide, guanidine, monoethanolamine, putrescine and piperazine.

Table S3. Calculated enthalpy ($\Delta H_{\text{heterodimer}}$ in kcal/mol), entropy ($\Delta S_{\text{heterodimer}}$ in cal/(mol·K)) and Gibbs free energy ($\Delta G_{\text{heterodimer}}$ in kcal/mol) for msa–base and na–base heterodimer formation at 298 K.

heterodimer	$\Delta H_{\text{heterodimer}}$	$\Delta S_{\text{heterodimer}}$	$\Delta G_{\text{heterodimer}}$
1msa1amm	−13.49	−30.84	−4.30
1msa1ma	−15.92	−28.72	−7.35
1msa1dma	−19.29	−35.39	−8.74
1msa1tma	−20.59	−35.40	−10.04
1msa1tmao	−29.73	−36.88	−18.74
1msa1gua	−26.55	−34.25	−16.34
1msa1mea	−21.05	−43.02	−8.22
1msa1put	−27.52	−46.82	−13.56
1msa1pz	−20.37	−36.86	−9.38
1na1amm	−12.12	−28.29	−3.69
1na1ma	−14.46	−33.49	−4.47
1na1dma	−15.74	−33.51	−5.75
1na1tma	−15.91	−33.99	−5.78
1na1tmao	−23.68	−35.13	−13.21
1na1gua	−20.49	−32.69	−10.74
1na1mea	−14.05	−32.35	−4.41
1na1put	−19.63	−41.40	−7.29
1na1pz	−16.44	−34.03	−6.29

Acidity measures

As a measure for acidity in the gas phase, we have calculated the proton affinities (PA) and gas acidities (GA) for each studied compound. The gas-phase reaction can be written as

$$\mathrm{BH^+} \rightarrow \mathrm{B} + \mathrm{H^+}. \tag{R1}$$

PA and GA are defined as the enthalpy and Gibbs free energy needed to extract a proton from the isolated gas-phase compound, respectively. That means the larger the PA and GA values are, the stronger the base is in the gas phase. For the bulk basicity, experimental $\mathrm{p}K_{\mathrm{a}}$ values are used (Haynes, 2014). A $\mathrm{p}K_{\mathrm{a}}$ value is a measure for the proton transfer ability when solvated by water, so it takes the solvation effect into account (Seybold and Shields, 2015). The larger the $\mathrm{p}K_{\mathrm{a}}$ value is, the stronger the base is in the aqueous phase. The aqueous-phase reaction can be written as

$$\mathrm{BH^+(aq)} \rightarrow \mathrm{B(aq)} + \mathrm{H^+(aq)}. \tag{R2}$$

The Gibbs free energy for the proton transfer reaction in the aqueous phase can be calculated from the experimentally determined $\mathrm{p}K_{\mathrm{a}}$ value as

$$\Delta G_{\mathrm{aq}} = \mathrm{p}K_{\mathrm{a}} RT \ln 10. \tag{2}$$

Table S4 shows different measures for acidities. As an alternative to Figure 4, the relationship between PA and $\Delta \mathrm{G}_{\text{heterodimer}}$ has been shown in Figure S3. In addition, the relationship between GA and $\Delta H_{\text{heterodimer}}$ is shown in Figure S3.

Table S4. Calculated proton affinity (PA) and gas acidity (GA), measured pK_a value from Haynes (2014) and aqueous-phase proton transfer free energy (ΔG_{aq}) and experimental PA and GA values from Hunter and Lias (1998). Values are given in kcal/mol at 298 K (when applicable).

Compound	PA (calc)	GA (calc)	pK_a	ΔG_{aq}	PA (exp)	GA (exp)
amm	203.7	195.5	9.3	12.6	204.02	195.75
ma	215.1	206.8	10.6	14.5	214.87	206.62
dma	222.6	214.6	10.7	14.6	222.16	214.27
tma	227.3	219.8	9.8	13.4	226.79	219.43
tmao	236.1	229.6	4.7	6.4	234.99	227.89
gua	236.0	227.6	13.6	18.6	235.73	226.91
mea	220.2	212.9	9.5	13.0	222.35	214.34
put	239.4	229.8	10.8	14.7	240.34	228.08
pz	226.9	219.3	9.7	13.2	225.55	218.62
sa	312.80	304.50	−3.0	−4.1	313.58	306.17
na	324.50	318.15	−1.4	−1.9	324.50	317.81
msa	319.98	313.92	−1.9	−2.6	320.98	315.01

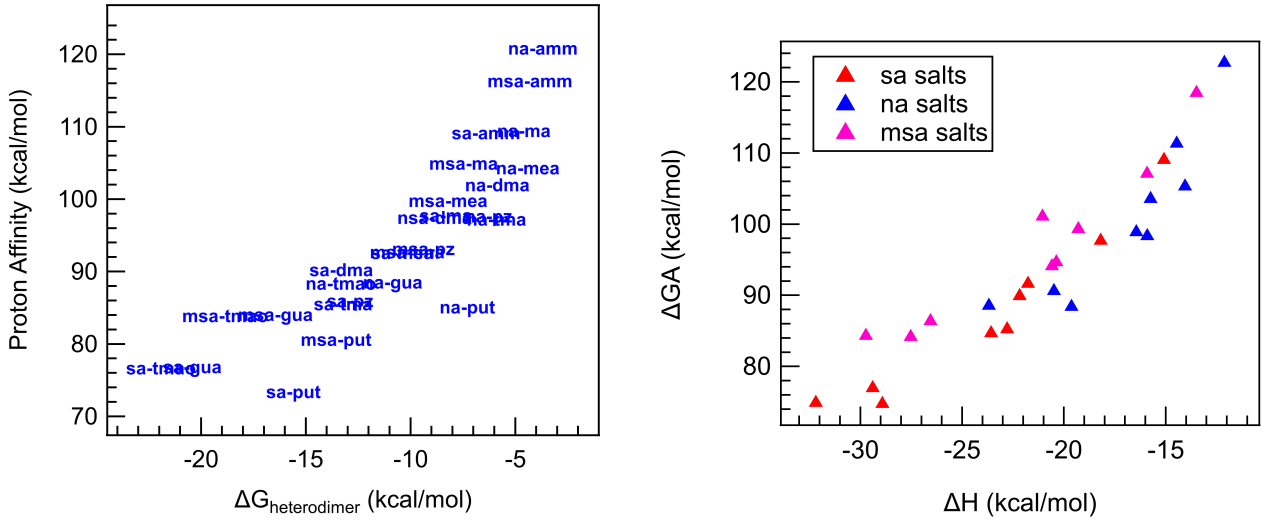

Figure S3. ΔPA plotted against $\Delta G_{heterodimer}$ (left) and ΔGA plotted against $\Delta H_{heterodimer}$ (right).

Base dipole moment and polarizability

In addition to base vapor pressure exhibiting no correlation with $\Delta G_{heterodimer}$, dipole moment and polarizability also show no relationship with heterodimer stability, as shown in Figure S4. Only sa salts are shown for clarity, as both neutral and cation forms of base polarizability and dipole moment are shown. Like vapor pressure, the only difference between the sa and na and msa salts would be a shift in $\Delta G_{heterodimer}$ for the same base polarizability or dipole moment values.

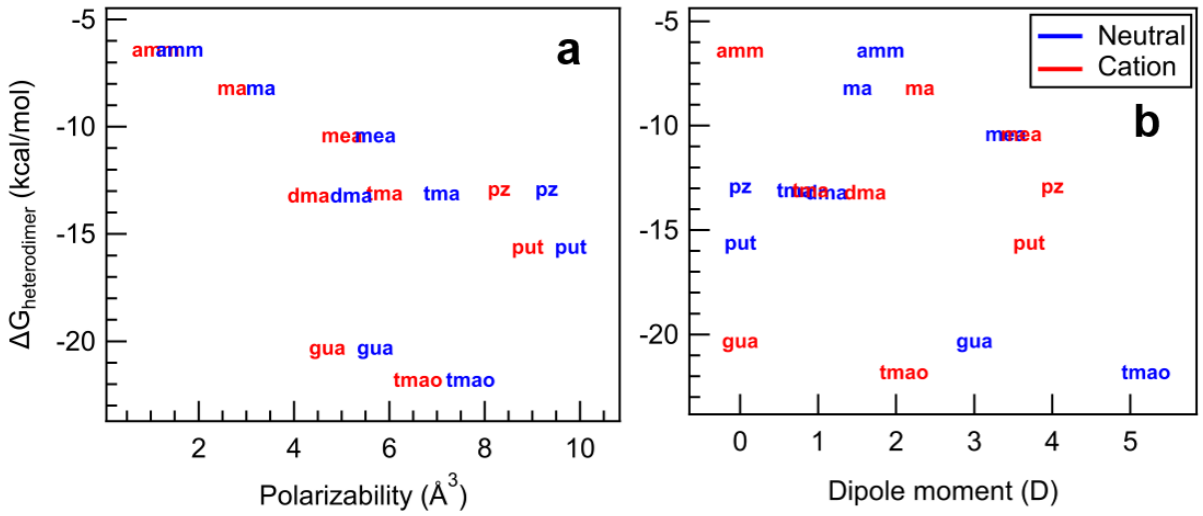

Figure S4. $\Delta G_{\text{heterodimer}}$ for sa–base salts plotted against base a) polarizability and b) dipole moment. Lack of correlation is seen in both plots, as also observed for base vapor pressure.

Boundary conditions in particle formation simulations

In NPF simulations, clusters are allowed to grow out of the 4acid4base simulation system as stable particles. The formed particle outside of a simulation box is expected to be stable in NPF simulations if it has larger or equal number of acid and base molecules than in following particles:

sa–amm: 5sa4amm
sa–ma: 5sa4ma
sa–dma: 5sa4dma
sa–tma: 5sa4tma
sa-tmao: 5sa3tmao and 4sa5tmao
sa–gua: 5sa4gua and 4sa5gua
sa–mea: 5sa3mea
sa–put: 5sa3put
sa–pz: 5sa3pz.

Simulated particle formation rates

Logarithm of the $J_{1.5}$ values for sulfuric acid–base systems with varying temperature and monomer concentrations are given in Table S5.

Table S5. Simulated $\log J_{1.5}$ values in $cm^{-3}s^{-1}$ for sa–base systems at varying temperature and monomer concentrations.

[A]=[B] (cm^{-3})	10^5	10^6	10^7	10^8	10^9	10^6	10^6	10^6	10^6
T (K)	298	298	298	298	298	248	273	323	348
amm	−40.0	−31.0	−22.0	−13.3	−5.0	−11.0	−20.9	−39.7	−47.1
ma	−25.1	−16.3	−8.0	−0.2	4.2	−5.1	−9.6	−24.6	−32.7
dma	−18.0	−9.1	−0.5	4.6	7.5	−0.4	−3.5	−18.1	−27.3
tma	−23.3	−15.3	−7.2	0.8	7.3	−0.9	−6.6	−23.8	−31.2
tmao	−9.7	−2.4	2.6	5.6	7.9	0.4	0.0	−6.2	−11.5
gua	−8.3	−0.5	3.6	5.8	7.9	−0.1	−0.2	−1.1	−4.7
mea	−21.0	−15.1	−6.5	0.5	5.6	−2.8	−6.8	−25.5	−34.6
put	−12.4	−4.5	2.6	5.8	7.9	0.5	0.0	−12.6	−20.4
pz	−16.1	−7.6	−0.2	4.6	7.4	−0.1	−2.9	−14.7	−23.1

The logarithm of the $J_{1.5}$ for sulfuric acid and ammonia or guanidine systems under all different conditions are given in Table S6.

Table S6. Simulated $\log J_{1.5}$ values in $cm^{-3}s^{-1}$ for sa–amm and sa–gua systems under all studied conditions.

amm	$\log J_{1.5}$	T (K)	[A]=[B] (cm^{-3})	gua	$\log J_{1.5}$	T (K)	[A]=[B] (cm^{-3})
	−19.8	248	10^5		−7.6	248	10^5
	−11.0	248	10^6		−0.1	248	10^6
	−3.1	248	10^7		3.7	248	10^7
	2.4	248	10^8		5.8	248	10^8
	5.9	248	10^9		7.9	248	10^9
	−29.9	273	10^5		−7.8	273	10^5
	−20.9	273	10^6		−0.2	273	10^6
	−12.3	273	10^7		3.7	273	10^7
	−4.2	273	10^8		5.8	273	10^8
	3.2	273	10^9		7.9	273	10^9
	−40.0	298	10^5		−8.3	298	10^5
	−31.0	298	10^6		−0.5	298	10^6
	−22.0	298	10^7		3.6	298	10^7
	−13.3	298	10^8		5.8	298	10^8
	−5.0	298	10^9		7.9	298	10^9
	−48.7	323	10^5		−9.1	323	10^5
	−39.7	323	10^6		−1.1	323	10^6
	−30.7	323	10^7		3.4	323	10^7
	−21.7	323	10^8		5.7	323	10^8
	−12.9	323	10^9		7.8	323	10^9
	−56.1	348	10^5		−13.3	348	10^5
	−47.1	348	10^6		−4.7	348	10^6
	−38.1	348	10^7		2.4	348	10^7
	−29.1	348	10^8		5.5	348	10^8
	−20.1	348	10^9		7.7	348	10^9

Hydrogen bonding in clusters

Hydrogen bonding rearrangement is shown in Figure S5 to demonstrate why H-bonds in the heterodimer were counted as the number of polar hydrogens on the molecule, as they are able to break and re-form new H-bonds to take part in subsequent cluster growth. For example, although putrescine (blue box) participates in H-bonding with itself to stabilize the heterodimer (1put1sa), the second amine group breaks those bonds to participate in H-bonds with the second sulfuric acid molecule in the 1put2sa cluster.

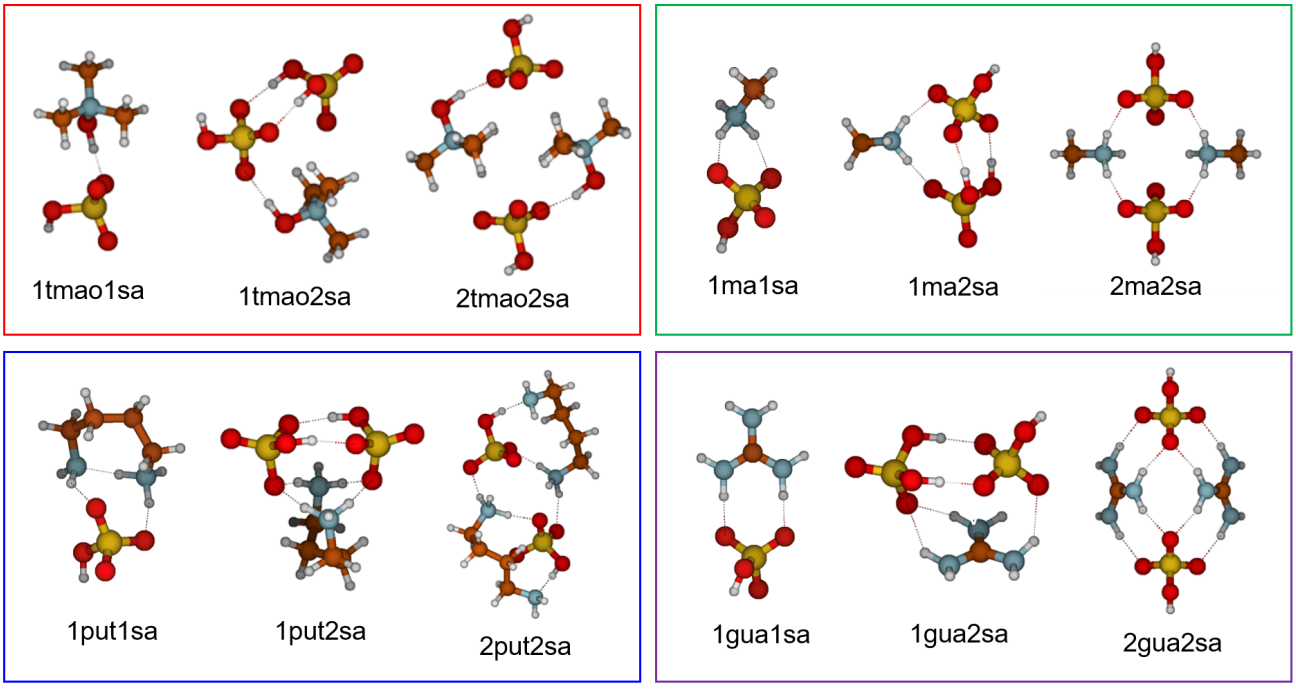

Figure S5. Molecular structures showing the H-bond rearrangement in 1base1acid, 1base2acid and 2base2acid clusters. Note that putrescine is doubly protonated in 1put2sa.

Predictive expressions of $J_{1.5}$ for ammonia

The fit lines in Figures 10 and 12a all follow the form:

$$J_{1.5} = A + B * \exp\left(-\frac{\log x - Constant}{C}\right), \tag{3}$$

where x is defined as either log[heterodimer] or Φ, and A, B, C, and Constant are fit coefficients, of which all values are defined in Table S7.

Table S7. Equation coefficients used for the trend lines plotted on Figures 10 and 12a, following equation 3.

	Condition		Equation Coefficients			
x	T (K)	[A] = [B] (cm^{-3})	A	B	C	Constant
log[heterodimer]	248	10^5–10^9	18.614	-38.569	7.0896	-2.554
	273	10^5–10^9	119.81	-149.72	31.973	-3.729
	298	10^5–10^9	300.62	-340.65	73.629	-4.704
	323	10^5–10^9	1528.6	-1577.3	348.09	-5.525
	348	10^5–10^9	14125	-14181	3148.9	-6.226
	248–348	10^5	91.754	-148.03	12.911	-6.226
	248–348	10^6	91.707	-138.98	12.075	-4.226
	248–348	10^7	67.519	-105.82	9.0243	-2.226
	248–348	10^8	30.158	-59.575	4.7254	-0.226
	248–348	10^9	15.175	-35.76	2.5685	1.774
Φ	248–348	10^5–10^9	92.237	-148.48	12.947	-1.726

The 21 sa–amm CLOUD $J_{1.7}$ data points that were compared to our predicted results are shown in Table S8, along with their respective experimental parameters and calculated $\Delta G_{heterodimer}$ values. Heterodimer concentration and Φ were calculated from this data for subsequent comparison to our model results.

Table S8. CLOUD data of the sa–amm system taken from Kirkby et al. (2011), with experimental conditions outlined, as well as J values used. Concentrations are in units of molec cm^{-3}, and rates are in units of cm^{-3} s^{-1}. $\Delta G_{heterodimer}$ values were calculated using Table S3 and the temperature of the respective CLOUD experiment, and are in units of kcal/mol.

T (K)	[sa]	[amm]	Ionization rate	RH(%)	$J_{1.7}$	log$J_{1.7}$	$\Delta G_{heterodimer}$
278.6	7.26E+08	7.64E+08	73.98	37.02	41.57	1.61878	-6.97364
278.6	7.48E+08	8.05E+08	3.24	37.01	3.36	0.526339	-6.96488
278.6	7.65E+08	8.69E+08	0	37	0.28	-0.55284	-6.96488
278.6	8.27E+08	1.29E+09	0	36.94	0.5	-0.30103	-6.97656
278.5	8.69E+08	9.84E+08	0	37.02	1.15	0.060698	-6.97364
278.5	3.86E+08	4.93E+08	3.63	37.37	0.06	-1.22185	-6.97656
278.3	4.42E+08	4.21E+08	2.4	38.37	0.65	-0.18709	-6.9678
278.3	8.55E+08	9.38E+08	2.01	37.56	3.52	0.546543	-6.96488
278.3	4.08E+08	3.34E+08	2.53	38.12	0.75	-0.12494	-7.84964
278.2	4.22E+08	4.59E+08	2.4	38.63	0.7	-0.1549	-6.97656
278.2	4.42E+08	4.98E+08	2.33	38.4	0.95	-0.02228	-7.84964
278.2	7.01E+08	5.95E+08	2.01	38.08	9.39	0.972666	-6.9678
278.2	4.28E+08	5.88E+08	2.27	37.97	1.05	0.021189	-6.97364
278.2	3.52E+08	5.91E+08	2.46	38.36	2.07	0.31597	-7.84964
278.2	4.45E+08	8.34E+08	2.53	38.07	1.03	0.012837	-7.84964
248.3	7.39E+07	6.57E+07	2.25	14.5	0.07	-1.1549	-6.97656
248.3	7.89E+07	6.57E+07	0	14.68	0.09	-1.04576	-7.84964
248.3	9.40E+07	1.22E+08	0	37.18	0.27	-0.56864	-6.96488
248.3	9.19E+07	1.22E+08	2.25	37.12	0.88	-0.05552	-6.97656
248.3	8.44E+07	6.59E+07	2.25	37.12	0.62	-0.20761	-6.97656
248.3	1.83E+08	1.22E+08	2.25	36.96	18.79	1.273927	-7.84964

Figure S6 shows the accuracy of using either the temperature or concentration expressions to predict the experimentally measured CLOUD values. The expression used to predict CLOUD data was determined based on the conditions of the experiment (i.e., if the experiment was run at 278 K, the 273 K equation was used, or if the experiment was run at starting monomer

concentrations approx. 10^8 molec cm^{-3}, the corresponding concentration equation was used). The use of monomer concentration expressions to predict J sees a larger spread in the predicted CLOUD $J_{1.7}$ rates: within 4 orders of magnitude compared to the temperature expressions predicting within 2 orders of magnitude. This stands to reason since the concentration equations are separated by an order of magnitude, which has more effect on J than steps of 25 K in temperature.

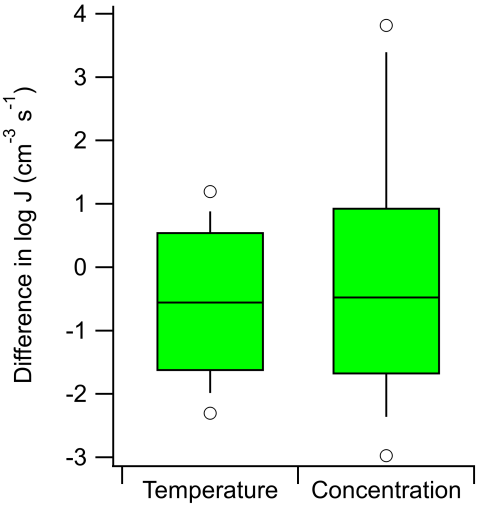

Figure S6. Differences between predicted and experimentally measured CLOUD $J_{1.7}$ values using either the temperature or concentration trend lines in Figure 10. Difference was defined to be $J_{\text{predicted}} - J_{\text{experimental}}$, with the box showing 75$^{\text{th}}$ percentiles, whiskers showing 95$^{\text{th}}$ percentiles, and open circles showing outlier data points.

References

Estimation Programs Interface Suite™ for Microsoft® Windows, v 4.11. United States Environmental Protection Agency, Washington, DC, USA.

Aston, B. J. G., Eidinoff, M. L., and Forster, W. S.: The Heat Capacity and Entropy, Heats of Fusion and Vaporization and the Vapor Pressure of Dimethylamine, Journal of the American Chemical Society, 61, 1539–1543, https://doi.org/10.1021/ja01875a061, 1939.

Aston, J. G., Siller, C. W., and Messerly, G. H.: Heat Capacities and Entropies of Organic Compounds. III. Methylamine from 11.5°K. To the Boiling Point. Heat of Vaporization and Vapor Pressure. The Entropy from Molecular Data, Journal of the American Chemical Society, 59, 1743–1751, https://doi.org/10.1021/ja01288a054, 1937.

Besel, V., Kubečka, J., Kurtén, T., and Vehkamäki, H.: Impact of Quantum Chemistry Parameter Choices and Cluster Distribution Model Settings on Modeled Atmospheric Particle Formation Rates, The Journal of Physical Chemistry A, 124, 5931–5943, 2020.

Haynes, W. M.: CRC handbook of chemistry and physics, CRC press, 2014.

Hunter, E. P. L. and Lias, S. G.: Evaluated Gas Phase Basicities and Proton Affinities of Molecules; Heats of Formation of Protonated Molecules, Journal of Physical and Chemical Reference Data, 27, 413–656, https://doi.org/10.1063/1.555719, 1998.

Kirkby, J., Curtius, J., Almeida, J., Dunne, E., Duplissy, J., Ehrhart, S., Franchin, A., Gagné, S., Ickes, L., Kürten, A., Kupc, A., Metzger, A., Riccobono, F., Rondo, L., Schobesberger, S., Tsagkogeorgas, G., Wimmer, D., Amorim, A., Bianchi, F., Breitenlechner, M., David, A., Dommen, J., Downard, A., Ehn, M., Flagan, R. C., Haider, S., Hansel, A., Hauser, D., Jud, W., Junninen, H., Kreissl, F., Kvashin, A., Laaksonen, A., Lehtipalo, K., Lima, J., Lovejoy, E. R., Makhmutov, V., Mathot, S., Mikkilä, J., Minginette, P., Mogo, S., Nieminen, T., Onnela, A., Pereira, P., Petäjä, T., Schnitzhofer, R., Seinfeld, J. H., Sipilä, M., Stozhkov, Y., Stratmann, F., Tomé, A., Vanhanen, J., Viisanen, Y., Vrtala, A., Wagner, P. E., Walther, H., Weingartner, E., Wex, H., Winkler, P. M., Carslaw, K. S., Worsnop, D. R., Baltensperger, U., and Kulmala, M.: Role of sulphuric acid, ammonia and galactic cosmic rays in atmospheric aerosol nucleation, Nature, 476, 429–433, https://doi.org/10.1038/nature10343, http://www.nature.com/articles/nature10343, 2011.

Matthews, J., Sumner, J. F., and Moelwyn-Hughes, E.: The Vapour Pressures of Certain Liquids, Transactions of the Faraday Society, 46, 797–803, 1950.

Seybold, P. G. and Shields, G. C.: Computational estimation of pKa values, WIREs Computational Molecular Science, 5, 290–297, https://doi.org/https://doi.org/10.1002/wcms.1218, https://onlinelibrary.wiley.com/doi/abs/10.1002/wcms.1218, 2015.

Stull, D. R.: Vapor Pressure of Pure Substances. Organic and Inorganic Compounds, Industrial & Engineering Chemistry, 39, 517–540, https://doi.org/10.1021/ie50448a022, 1947.

Swift, E. and Hochanadel, H. P.: The Vapor Pressure of Trimethylamine from 0 to 40°, Journal of the American Chemical Society, 67, 880–881, https://doi.org/10.1021/ja01221a508, 1945.